Colloidal PbS Quantum Dot Solar Cells with High Fill Factor

Ni Zhao,[†] Tim P. Osedach,[†,‡] Liang-Yi Chang,[§] Scott M. Geyer,[§] Darcy Wanger,[§] Maddalena T. Binda,[⊥] Alexi C. Arango,[†] Moungi G. Bawendi,[§] and Vladimir Bulovic[†,*]

[†]Department of Electrical Engineering and Computer Science, Massachusetts Institute of Technology, Cambridge, Massachusetts 02139, [‡]School of Engineering and Applied Sciences, Harvard University, Cambridge, Massachusetts 02138, [§]Department of Chemistry, Massachusetts Institute of Technology, Cambridge, Massachusetts 02139, and [⊥]Department of Electronics and Information Technology, Politecnico of Milan, Milan, Italy

ABSTRACT We fabricate PbS colloidal quantum dot (QD)-based solar cells using a fullerene derivative as the electron-transporting layer (ETL). A thiol treatment and oxidation process are used to modify the morphology and electronic structure of the QD films, resulting in devices that exhibit a fill factor (FF) as high as 62%. We also show that, for QDs with a band gap of less than 1 eV, an open-circuit voltage (V_{OC}) of 0.47 V can be achieved. The power conversion efficiency reaches 1.3% under 1 sun AM1.5 test conditions and 2.4% under monochromatic infrared ($\lambda = 1310$ nm) illumination. A consistent mechanism for device operation is developed through a circuit model and experimental measurements, shedding light on new approaches for optimization of solar cell performance by modifying the interface between the QDs and the neighboring charge transport layers.

KEYWORDS: lead sulfide · quantum dot · fullerene · photovoltaic · solar cell · air annealing · recombination

Over the past several decades, intensive research efforts have been undertaken to develop low-temperature processed photovoltaic cells through the use of nanostructured materials including small molecules,[1−4] conjugated polymers,[5−9] and colloidal nanocrystal quantum dots (QDs).[10,11] There has been much progress in improving the power conversion efficiency (PCE) of nanostructured solar cells in the visible light region with reported efficiencies reaching 6.7%.[5,9] An important approach toward realizing significant improvements to this performance is to extend the spectral sensitivity of cells to near-infrared wavelengths, which contain as much as half of the energy of the solar spectrum. This can potentially be achieved by using colloidal nanocrystal QDs as the light-harvesting material, as their optical band gap can be tuned to a desired range by choosing the appropriate material composition and by controlling nanocrystal size during synthesis.[12−14]

Among the QD materials, PbS and PbSe QDs possess excellent photosensitivity in the near-infrared spectrum. Solar cells based on a Schottky barrier formed at the interface of the p-type PbS or PbSe QD films and a metal cathode have been reported[15−18] with PCEs of up to 2.1%[15] under 1 sun AM1.5 test conditions. In these devices, it is suggested that photocurrent is generated by field-assisted charge separation in the depletion region. One limitation of Schottky-based solar cells is that the open-circuit voltage (V_{OC}), an important metric that directly affects the PCE, is expected to be lower than 0.5 E_g/q,[19] where E_g is the band gap of the semiconducting material and q is the electron charge. A heterojunction solar cell incorporating an electron-transporting/hole-blocking layer between the QDs and the metal cathode could potentially allow for a higher V_{OC}. The challenge in realizing such a device is to find materials that provide an appropriate energy level alignment with the low band gap QDs such that electron injection from QDs to the material is promoted while back electron transfer to the QDs (that would lead to the undesirable electron−hole recombination) is suppressed. Recently, Choi *et al.*[20] and Leschkies *et al.*[21] separately reported a high-efficiency excitonic solar cell structure composed of a PbSe QD layer sandwiched between a ZnO electron-transporting layer (ETL) and an organic hole-transporting layer. In order to achieve a V_{OC} of 0.45 V, small QDs with relatively large band gaps (E_g = 1.3−1.4 eV) were required, limiting the infrared solar spectral range harvestable by these cells. Also, the introduction of the ETL layer did not seem to improve the fill factor (FF) of the solar cells, which remained at 30−40%, similar to those of the Schottky solar cells. In the present work, we demonstrate that it is possible to improve both the V_{OC} and the FF of QD/ETL bilayer solar cells through

*Address correspondence to bulovic@mit.edu.

Received for review January 21, 2010 and accepted June 22, 2010.

Published online June 30, 2010.
10.1021/nn100129j

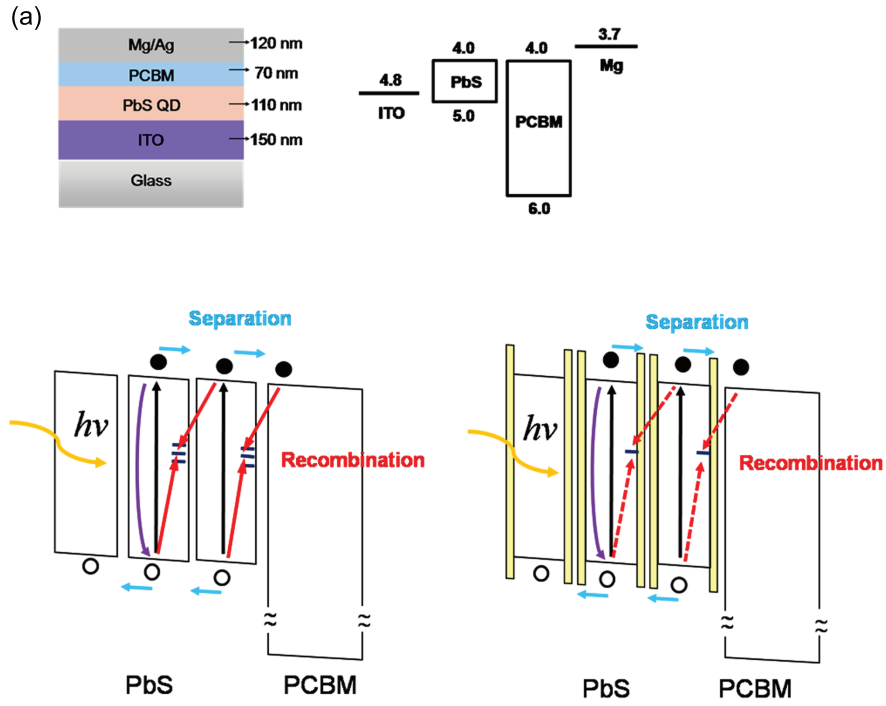

Figure 1. (a) Schematic of the bilayer solar cell structure and the energy level diagram of device components referenced to the vacuum level. (b) Illustration of the charge flow mechanism in the pristine (left) and air-annealed (right) PbS QD/PCBM devices. The black arrows denote the exciton generation process, the purple arrows denote the geminate electron−hole pair recombination process, the blue arrows denote the charge separation process, and the red arrows denote the bimolecular recombination process (assisted by midgap states). The thin wider band gap layers (yellow) that surround each QD in the right figure represent the oxide compounds, and the dashed red arrows indicate a suppressed charge recombination *via* the bimolecular process. Note that the charge separation and recombination occur in both the bulk PbS QD layer and at the PbS QD/PCBM interface.

modifying the interface properties that govern the charge separation and recombination process in these devices.

The bilayer QD/organic solar cells presented in this study consist of an ITO-coated glass substrate on which we deposit a thin film of PbS QDs (fabrication details are presented in the Methods section), which acts as both the light-absorbing and charge-transporting layer. The QD film is then coated with a thin film of a fullerene derivative, [6,6]-phenyl-C61-butyric acid methyl ester (PCBM), which serves as the electron-transporting and hole-blocking layer. (PCBM was chosen in this work because efficient electron transfer from PbS QDs to PCBM was demonstrated in a recent study of PbS QD/PCBM photodetectors.[22,23]) To modify the electronic structure of individual PbS QDs and QD thin films in our devices, the QD films are subjected to air annealing, nitrogen annealing, or ozone exposure. Air annealing has previously been used to improve the conductivity of QD films *via* a doping mechanism.[24,25] It has also been shown to enhance the V_{OC} and the air stability of PbS QD-based Schottky devices,[26,27] where chemical analysis revealed that the performance improvement is related to the formation of PbO and $PbSO_3$ during the air annealing process. However, the mechanism through which these oxidation products affect the charge separation, recombination, and transport remains unclear.

Here, for solar cells containing small band gap PbS QDs ($E_g < 1.0$ eV) that are air-annealed and treated with thiols prior to PCBM deposition, we measure a fill factor as high as 62%. Also, a V_{OC} of 0.47 V is achieved for QDs with a band gap of 0.97 eV (after air annealing). This exceeds the V_{OC} value of 0.27 V predicted by the relation $V_{OC} = 0.6\ (E_g/e) - 0.31$ as reported in PbSe/ZnO heterojunction solar cells.[21] The PCE for these structures is ~1.3% under 1 sun AM1.5 test conditions and 2.4% under monochromatic infrared light illumination (of wavelength $\lambda = 1310$ nm, corresponding to $E = 0.95$ eV). We also demonstrate that further improvement of the PCE is possible with ozone treatment (reaching a PCE of 1.7% under AM1.5, but with lower V_{OC} and FF). Devices made with and without oxidation treatments are studied through measurements of optical absorption, quantum efficiency, shunt and series resistances, light intensity dependence, and charge recombination lifetime. The results suggest that the use of the bilayer structure and the oxidation treatment enhances the shunt resistance of the device by suppressing the charge recombination process, resulting in a high V_{OC} and FF.

RESULTS AND DISCUSSION

Device Performance. A schematic of our device structure is shown in Figure 1a. The long oleic acid ligands

on the as-synthesized QDs were first replaced by butylamine ligands in solution, which were then exchanged by ethanedithiol ligands (detailed procedure is described in the Methods section) after formation of QD films to improve charge transport properties and decrease solubility of the films. The QD layer is then processed in one of four different ways prior to the deposition of PCBM: no further treatment (pristine), annealed in air (air-annealed), or nitrogen atmosphere (N_2-annealed) at 110 °C for 30 min, or treated in an ozone environment for 6 s (ozone-treated). For the annealed devices, we applied a post-annealing ethanedithiol (EDT) solution treatment to the QD layer for 30 s, which has been observed to lead to a higher photocurrent in our PbS QD/PCBM devices. Notably, this treatment has the effect of reducing the conductivity of air-annealed films of PbS QDs (see the measurements on charge transport in QD films in the Supporting Information, Figure S1), presumably due to it passivating surface states on QDs and therefore reducing the carrier concentration. Meanwhile, the increase of the photocurrent in the solar cell devices indicates that the post-annealing treatment may increase the exciton lifetime and reduce the density of electron traps in PbS QDs, which should increase electron transfer to the PCBM film.

The current−voltage ($I-V$) characteristics of these devices in the dark and under simulated AM1.5 test conditions are plotted in Figure 2a,b, respectively, and the photovoltaic parameters of merit are summarized in Table 1. We note that the air annealing procedure leads to a substantial increase in both the V_{OC} and the FF. Nitrogen annealing had no such positive effect, suggesting that the enhancement of the device performance is related to an oxygen-induced reaction in air.

In addition to air annealing, ozone treatment of as-deposited QD films also enhances the V_{OC} and FF. The increase in the photocurrent of the device after the ozone treatment leads to the highest power conversion efficiency among all of the devices studied here. Compared to air annealing, in which samples are subjected to an elevated temperature for 30 min, a short room-temperature treatment in ozone (6 s long) allows for a rapid surface oxidation process that should facilitate removal of QD capping ligands and formation of an oxide shell for QDs, particularly those at the top surface of the QD film, which form a heterojunction with the PCBM overlayer. Longer ozone exposure results in a decreased J_{SC} and an increased V_{OC}. In the analysis that follows, we largely focus on the differences between the pristine and the air-annealed bilayer devices as the latter exhibit the highest V_{OC} and fill factor and contain a more uniformly oxidized QD film as compared to ozone-treated devices.

Composition Change during Air Annealing. In order to investigate changes in the chemical composition of the PbS QD films, X-ray photoelectron spectroscopy (XPS) was carried out on the pristine film and on the air-annealed films before and after post-annealing EDT treatment. The XPS spectra show the presence of Pb, S, C, and O. The atomic ratios of these elements in different samples are summarized in Table 2. As expected, air annealing increases the concentration of oxygen. Following the post-annealing EDT treatment, the oxygen concentra-

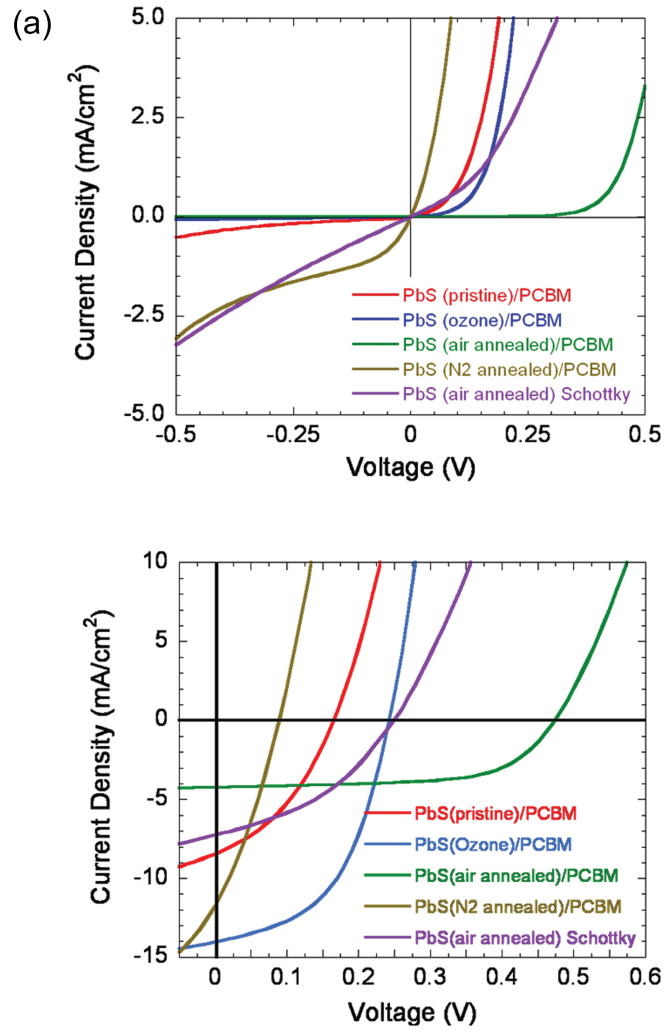

Figure 2. Current−voltage characteristics of representative solar cells (a) in the dark and (b) under 100 mW/cm² AM1.5 illumination.

TABLE 1. Response of PbS QD/PCBM Solar Cells under Simulated AM1.5 (100 mW/cm²) Illumination[a]

PbS QD PVs	J_{SC} (mA/cm²)	V_{OC} (V)	FF (%)	PCE (%)	R_S (Ω cm²)	R_{SH} (Ω cm²)
N_2-annealed	11.7	0.085	32	0.32	1.5	40
pristine	8.2	0.16	38	0.50	2.1	530
ozone-treated	14.0	0.24	50	1.68	1.7	3200
air-annealed	4.2	0.47	62	1.27	16.4	120000
Schottky (air-annealed)	7.2	0.25	38	0.68	20	180

[a]The devices are listed in the order of increasing V_{OC} and FF. Response of the Schottky PbS QD/Mg solar cells is also indicated. The series (R_S) and shunt resistance (R_{SH}) are calculated from $\partial V/\partial J$ at $V = 0.5$ V and $V = -0.1-0$ V, respectively, for each $J-V$ curve of devices in the dark.

TABLE 2. XPS Chemical Composition (atom %) of the PbS QD Films

films	Pb	S	C	O
pristine	34.7	33.6	30.2	1.5
air-annealed (without EDT)	23.1	19.3	29.8	27.8
air-annealed (with EDT)	21.9	25.7	35.6	16.8

[a]The "with EDT" and "without EDT" refer to with and without post-annealing EDT treatment, respectively.

tion is observed to decrease. Concentrations of carbon and sulfur, on the other hand, are observed to increase. To more precisely identify the species formed during the chemical treatments, we focused on the XPS spectra of S 2p and O 1s peaks (Figure 3). Peak fitting of line shapes to the spectra reveals the presence of PbO, $PbSO_3$, and $PbSO_4$ in PbS QD films after air annealing (refer to Figures S1 and S2 and Table S1 in Supporting Information for detailed analysis). Post-annealing EDT treatment reduces the amount of these oxide compounds and changes their relative composition. For instance, the molar ratio between $PbSO_3$ and $PbSO_4$ changes from 1:1.3 to 1:0.7, suggesting a greater reduction in the $PbSO_4$ composition after EDT treatment. This agrees with the earlier study by Konstantatos *et al.*,[28] which showed that thiol treatment can remove the $PbSO_4$ on the surface of QDs while leaving behind $PbSO_3$. As noted earlier, our annealing condition leads to a relatively aggressive oxidation process. Rather than only modifying the surface chemistry of the QDs, as in the case of a solution-phase treatment[28] or short air annealing process,[24] it converts a considerable amount of PbS (~40%) to amorphous oxide compounds that surround the QDs. The benefits of creating this morphology will be discussed later. Besides modifying the composition of the oxide compounds, the post-annealing EDT treatment also increases the relative concentration of C−S (thiol) species, indicative of surface trap passivation by EDT ligands. Henceforth, a post-annealing EDT treatment is implied for devices described as having been "air-annealed" or "N_2-annealed", unless otherwise specified.

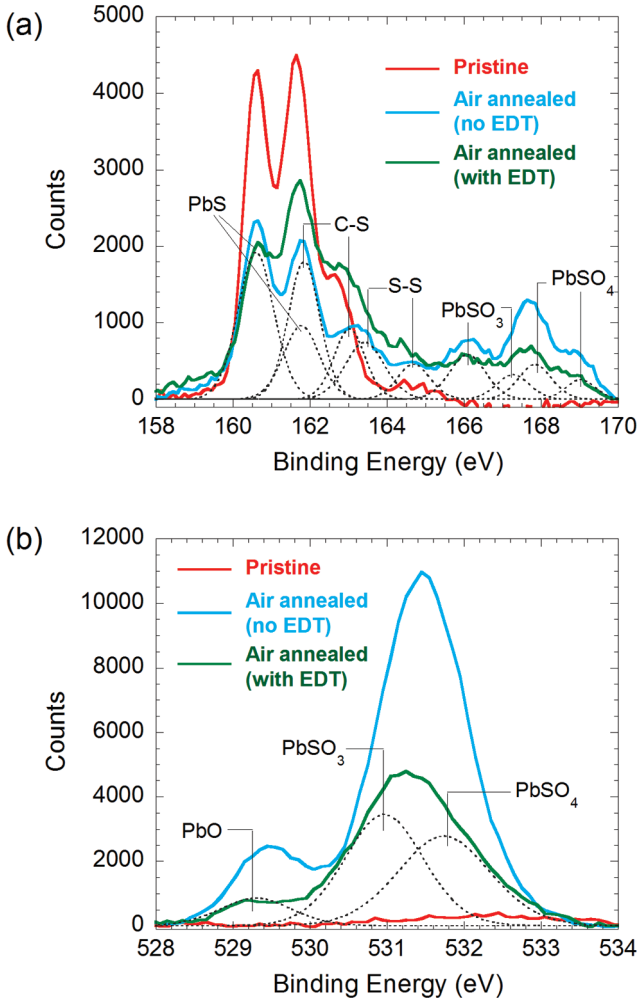

Figure 3. XPS spectra of S 2p (a) and O 1s (b) peaks in pristine (red) QD film and air-annealed QD films with (green) and without (cyan) EDT post-annealing treatment. Sulfur species are fitted with a S 2p doublet (dotted line) with a 2:1 intensity ratio and 1.18 eV splitting energy. The binding energies for the species are 160.6 and 161.78 eV for PbS, 161.85 and 163.03 eV for C−S, 163.43 and 164.61 eV for S, 166.10 and 167.28 eV for $PbSO_3$, and 167.84 and 169.02 eV for $PbSO_4$. Oxygen species are fitted with an O 1s singlet (dotted line). The binding energies for the species are 529.3 eV for PbO, 530.96 eV for $PbSO_3$, and 531.7 eV for $PbSO_4$.

Absorption Spectra of QD Films. Changes in the structure of the PbS QD films upon ozone, air, and nitrogen treatments are readily observed in their optical absorption spectra (Figure 4a). The pristine film and the ozone-treated film show nearly identical absorption features, suggesting that the brief ozone treatment only oxidizes a very small portion of the QDs (presumably those near the film surface) and that the light absorption in the film is dominated by the unoxidized QDs. During air annealing, the surface of the PbS QDs reacts with oxygen to form oxide compounds, as shown in the XPS measurement. The oxide compounds remain as an amorphous matrix around the QDs (as indicated in the band structure diagram of Figure 1b), while the effective size of the QDs becomes smaller. For our QD films, the spectrum of the air-annealed film exhibits the first excitonic transition at $\lambda = 1280$ nm, about 170 nm blue-shifted from the corresponding absorption peak of the pristine film, which indicates a 0.1 eV increase in the band gap of the air-annealed QDs. This corresponds to a reduction of 0.8 nm in QD diameter, which is consistent with the value extracted from X-ray diffraction data of the films (see Supporting Information, Figure S3). According to the QD size dependence of V_{OC} reported in other publications,[15,20,21] such QD size reduction can lead to 0.05 V increase in the V_{OC}, which is insufficient to explain the larger increase (0.3 V) in V_{OC} that we observe after air annealing of pristine QD films (see Table 1 and Figure 2b). For comparison, the absorption spectrum of the nitrogen-annealed film is also plotted in Figure 4a, which, in contrast, has its first excitonic peak slightly red-shifted relative to the peak of the pristine film. This is consistent with a densification of QD films

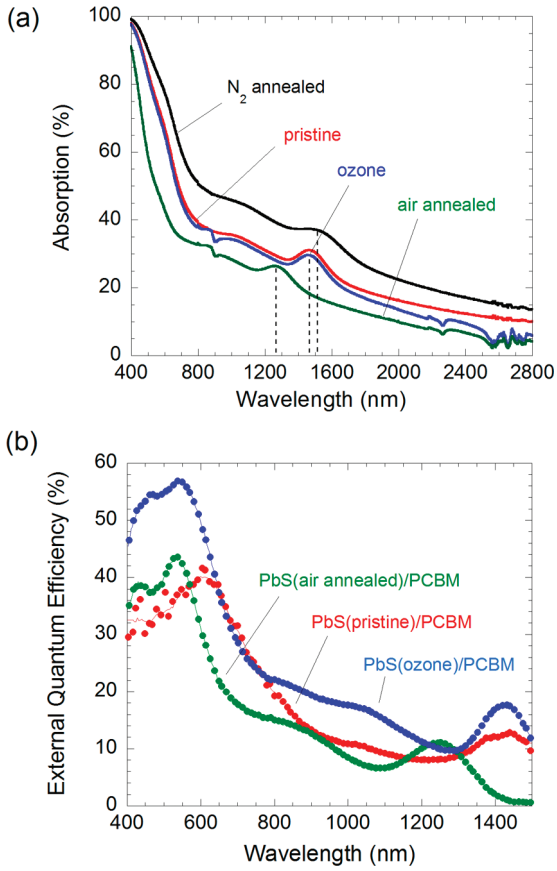

Figure 4. (a) Optical absorption spectra of discrete PbS QD films under different processing conditions. (b) External quantum efficiency (EQE) spectra of PbS QD/PCBM devices.

as the nitrogen anneal introduces slight sintering and causes a solvatochromic effect,[29] both of which would lead to the observed absorption red shift.

Besides the shift in the first excitonic transition peak, the total light absorption of the PbS QD film is also reduced after air annealing, due to part of the PbS reacting with oxygen to form wider band gap oxides, which lowers the concentration of the optically absorptive PbS. Figure 4b shows the external quantum efficiency (EQE) of the pristine, air-annealed, and ozone-treated devices as a function of wavelength, showing a diminished photoresponse intensity in the air-annealed devices, reflecting the lower absorption fraction for these structures, as measured in Figure 4a.

Shunt and Series Resistance. Differences in the performance of the devices can be analyzed using a standard equivalent circuit model (inset in Figure 5), from which we extract the series resistance (R_S) and the shunt resistance (R_{SH}) of each device in the dark (values tabulated in Table 1). We note a strong correlation between the V_{OC} and FF and the shunt resistance R_{SH} (Figure 5), with V_{OC} and FF of a device increasing for larger R_{SH}. The finite value of R_{SH} reflects the presence of current leakage paths through the solar cells and/or bimolecular recombination of charge carriers within the solar cells. The air annealing process can efficiently enhance R_{SH}

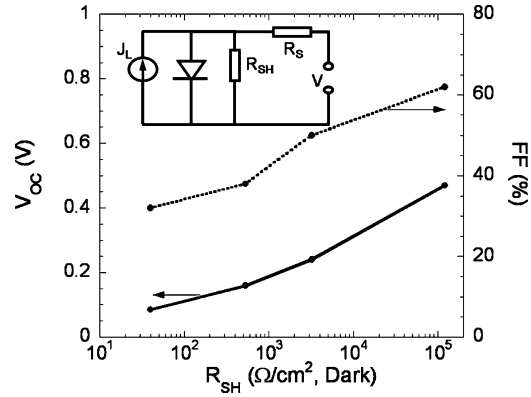

Figure 5. Open-circuit voltage (V_{OC}, solid line) and fill factor (FF, dashed line) plotted against the derived values of shunt resistance R_{SH}. Inset: Equivalent circuit model of a solar cell.

as it can not only form an insulating matrix surrounding the QDs that reduces the leakage current but also provide an energy barrier that suppresses the bimolecular recombination process (Figure 1b).

In contrast to R_{SH}, the variation in R_S among the tested devices is relatively small between the light/dark conditions. R_S is 10-fold higher in the air-annealed devices (both heterostructure and Schottky) as compared to the pristine, nitrogen, or ozone-treated solar cells, which reflects the reduction in charge mobility in the air-annealed QD films, due to the oxide growth on the PbS QDs. Although these wide band gap oxides in PbS QD films lead to a higher R_S, they also increase R_{SH} (Figure 1b), which, in turn, leads to the higher V_{OC} and FF. In contrast, nitrogen-annealed PbS QD films have a low R_S and consequently a higher J_{SC}. However, nitrogen-annealed PbS QD films fail to produce high a R_{SH}, leading to lower V_{OC} and FF.

Besides R_{SH}, we found that the V_{OC} is also strongly correlated to the turn-on point of the forward current in the dark (Figure 2a). This result is not surprising as V_{OC} corresponds to the situation where the photocurrent is completely balanced by the dark current. Therefore, for a fixed photocurrent, a late turn-on of the device in the dark will lead to a high V_{OC}. In our devices, the turn-on occurs when recombination of injected electrons and holes prevails in the forward bias. Hence a device with diminished charge recombination rate (*i.e.*, device that can build up a larger quantity of separated charges) would yield a high V_{OC}.

Comparing Bilayer and Schottky Solar Cells. The benefit of incorporating a PCBM layer into the photovoltaic structure is evident from the comparison of the air-annealed PbS QD/PCBM bilayer device with a Schottky solar cell consisting of just the air-annealed PbS QD layer in direct contact with the Mg/Ag cathode. The R_S for both structures is nearly the same, indicating that the PCBM film does not dominantly contribute to the series resistance of these cells. The V_{OC} and FF are higher in the bilayer device, reflecting a higher charge buildup and smaller leakage. The Schottky device, however, exhibits a larger

short-circuit current (J_{SC}), which can result from a wider depletion region for exciton dissociation[15,17] and/or a higher efficacy of exciton dissociation at the QD/cathode interface due to the reduced charge buildup. It is also notable that in our experiments the device yield and reproducibility are much higher in the bilayer device structure, presumably due to the PCBM layer effectively blocking metal penetration through the QD layer during the evaporation of the top electrode, reducing leakage paths and yielding a more reproducible electron transfer interface.

The effect of bimolecular recombination on V_{OC} can also be seen by comparing the performances of the pristine bilayer device and the air-annealed Schottky device: The former has a lower leakage current (as shown in Figure 2a) and a higher R_{SH}; however, its V_{OC} is lower than the air-annealed Schottky device. This suggests that reducing the leakage current alone is not sufficient to achieve a high V_{OC} and that suppression of charge recombination is vital in the bilayer devices.

Light Intensity Dependence and Charge Transport. The current−voltage characteristics of the devices were measured under monochromatic infrared (IR) light illumination ($\lambda = 1310$ nm) of different intensities, where PCBM is transparent for the selected wavelength of IR light, ensuring that all of the photogeneration is taking place in the PbS QD film. We observe that the high V_{OC} and FF are maintained in the IR-illuminated air-annealed devices (Figure 6a), and that the IR power conversion efficiency reaches 2.4%. This not only confirms that the shape of the $I-V$ characteristics is determined by the PbS QD layer but also proves that such devices can be used to efficiently harvest the IR portion of sunlight.

The light intensity dependence of the normalized short-circuit current density (J_{SC}) under IR illumination is plotted in Figure 6b for the pristine, air-annealed, and ozone-treated devices. The experimental data are fitted with $J_{SC} \propto I^{\alpha}$ to ascertain the contribution of charge recombination in the loss mechanism for the photocurrent. It has been predicted that $\alpha = 1$ when the photocurrent is determined by the generation rate of electron−hole pairs upon photon absorption, while $\alpha = 0.75$ when the photocurrent is further limited by formation of space-charge regions due to unbalanced charge transport for electron and holes.[30] In our experiment, $\alpha = 0.96$ for the pristine and ozone-treated device and $\alpha = 0.81$ for the air-annealed device, suggesting that the air annealing treatment and subsequent post-annealing thiol treatment limit the charge transport properties of the PbS QD film, leading to a space-charge effect. To elucidate this point, we measured charge transport through the PbS QD films in a field-effect transistor (FET) geometry and found that the hole mobility in the QD film decreases from 5.0×10^{-3} to 5.5×10^{-5} cm^2/V·s after air annealing/thiol post-annealing treatment (mobility values are extrapolated from the FET characteristics in the linear regime; see Figure S4 in the Supporting Information). The decrease in the film mobility can again be attributed to the insulating oxide compounds acting as a barrier for charge transport. The fact that the fill factor increases after air annealing shows that the bias dependence of the photocurrent is much less affected by the reduced charge transport than it is by the increased shunt resistance, which would suggest that the initial geminate pair separation is very efficient in the QD films.

Figure 6b also shows the increase in V_{OC} for the three types of devices with the increasing IR light intensity. The increase of V_{OC} with intensity is the largest for the air-annealed devices, which can be attributed to a low recombination rate of the photogenerated charges in these structures. In contrast, faster recombination in the pristine PbS QD films leads to rapid depletion of the separated photogenerated charge and hence a lower increase of the V_{OC} with light intensity. The ozone-treated devices represent an intermediate situation. It is likely that in these devices only the interface QDs are oxidized. Therefore, the increase in their V_{OC} values, as compared to the pristine devices, would originate from the reduced charge recombination at the QD/PCBM heterointerface, while the decrease of the V_{OC} in the ozone-treated devices, as compared to the air-annealed devices, reflects the fast charge recombination in the unoxidized bulk QD films. The direct measurement of the charge recombination rates for different structures is discussed in the next section.

Charge Carrier Recombination Life Time. To directly measure charge recombination in the PbS QD/PCBM bilayer solar cells, we performed small perturbation transient open-circuit voltage decay measurements.[31−33] In this measurement, a DC-biased IR light source ($\lambda = 1310$ nm) is used to illuminate the device to create excitons that dissociate into electrons and holes. The separated carriers fill up the sub-band gap states between the conduction and valence band edges and increase the distance between the quasi-Fermi levels for electrons and holes, E_{Fn} and E_{Fp}, respectively. In an open-circuit condition, this is manifested as the measured V_{OC}. Simultaneously, a low-intensity pulsed IR light is used to induce a small perturbation to the V_{OC} by transiently generating additional electrons and holes. This leads to a small and momentary increase in the energy difference between E_{Fn} and E_{Fp}. The resulting additional transient photovoltage, ΔV, will then decay with a lifetime τ that is determined by the recombination rate constant (k_{rec}, $\tau = 1/k_{rec}$) of the electrons and holes. Figure 7a shows the transient voltage decay curves of pristine and air-annealed devices, which can both be fitted to a monoexponential decay function to extract the lifetime τ and consequently the k_{rec}.

In Figure 7b, we plot k_{rec} as a function of the DC-biased light intensity. For all the devices, k_{rec} increases with increasing light intensity. This is expected as the

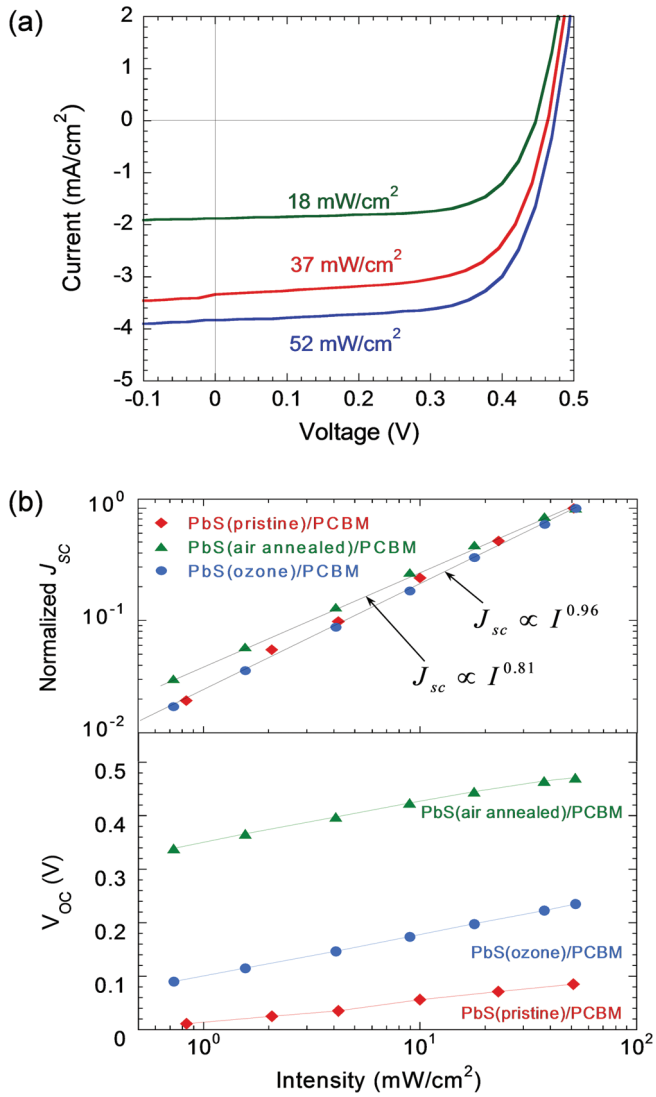

Figure 6. (a) Current−voltage characteristics of an air-annealed device under monochromatic IR illumination (λ = 1310 nm) at different intensities. (b) (Top) Incident light intensity dependence of the normalized short-circuit current (J_{SC}) for PbS QD/PCBM devices. The experimental data (symbols) are fitted (solid lines) using $J_{SC} \propto I^{\alpha}$. (Bottom) Incident light intensity dependence of the open-circuit voltage (V_{OC}).

mobility of charge carriers is improved as more traps become filled by photogenerated charge carriers and the improved mobility can consequently increase the charge recombination rate constant by increasing the frequency of opposite charge carriers encountering each other. We observe that the air-annealed device exhibits a k_{rec} much smaller than the pristine and ozone-treated device at low light intensities, indicating that at low photogenerated charge carrier concentrations the charge loss due to recombination process is greatly suppressed in the air-annealed device. The reduced charge loss compensates the reduction of photogenerated carriers at low light intensities, which explains the maintaining of high V_{OC} in the air-annealed device at such conditions. The correlation of k_{rec} and V_{OC} is plotted in Figure 7c. For the pristine devices, even at low V_{OC}, k_{rec} is relatively large, hampering a steady-state accumulation of separated photogenerated charge. For the air-annealed devices, a similarly high k_{rec} is only observed at much larger values of V_{OC} when a significant amount of photogenerated charge is separated.

On the basis of the above observations, we propose a model (Figure 7d) to explain the charge recombination process in our devices at an open-circuit condition. In the air-annealed device, a thin layer of oxide compounds at the PbS QD/PCBM interface can act as a barrier for charge recombination. At low light intensities, there is only a small amount of photogenerated carriers available to fill up the subgap states. Therefore, the position of the electron Fermi level is low, and the activation energy required for charge carrier recombination is high, resulting in a low k_{rec}. As the light intensity increases, more subgap states are filled with photogenerated electrons, which further raises the electron Fermi level and accelerates the charge recombination process until, eventually, the electron transfer from the

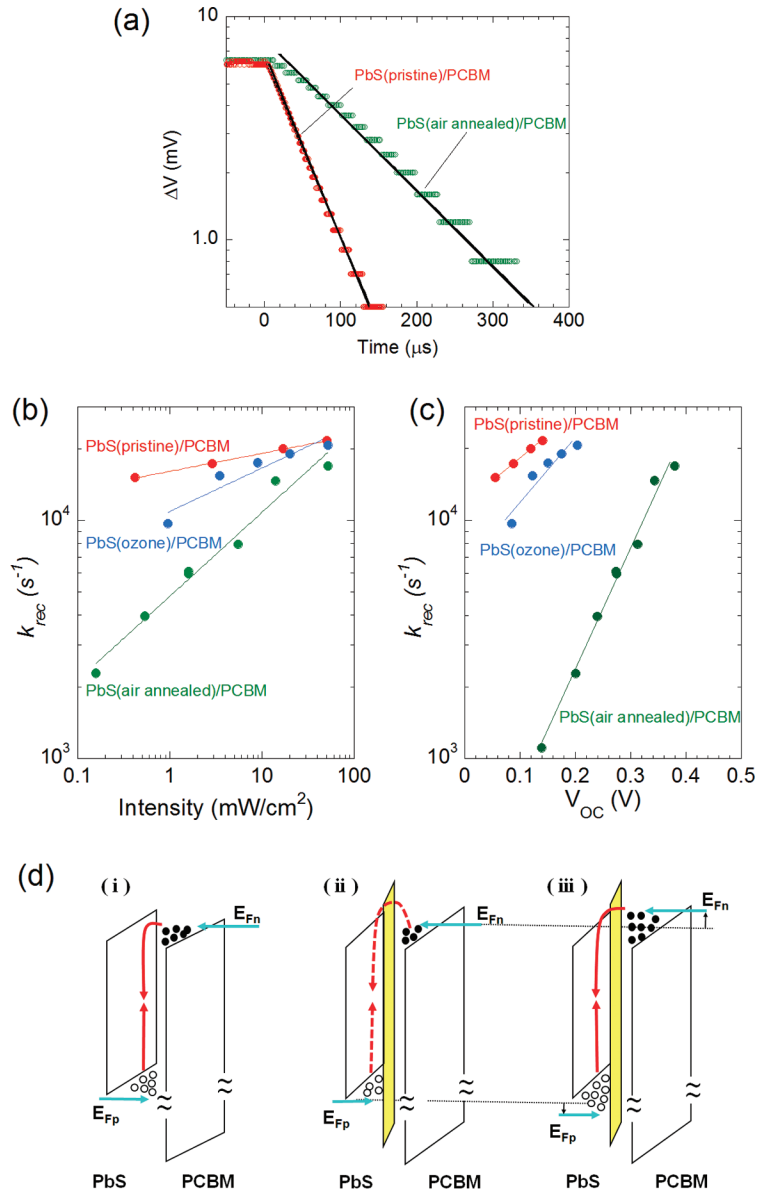

Figure 7. (a) Typical transient photovoltage (ΔV) decay data together with a monoexponential decay function fit at 0.5 mW/cm^2; (b) k_{rec} *vs* light intensity and (c) k_{rec} *vs* V_{OC} measured for the pristine, ozone-treated, and air-annealed devices. (d) Charge recombination process in the devices at an open-circuit condition for a pristine device (i) and an air-annealed device at low light intensity (ii) and at high light intensity (iii). The red arrows denote charge recombination process, with the solid and dashed lines indicating fast and slow recombination rates, respectively. Note that the mechanism also applies to the bulk PbS QD layer between a QD donor and a QD acceptor.

PbS QD to PCBM is matched by the back electron transfer, thus pinning the photovoltage. In this situation, the V_{OC} saturates and the k_{rec} probed by the transient V_{OC} measurement reflects the recombination rate constant within the QD film. For the pristine device, since there is minimal oxide barrier at the PbS QD/PCBM interface, the charge recombination can occur relatively easily even at low light intensities and the electron Fermi level can only move a small amount before the back electron transfer limits the photogeneration process, leading to a low maximum V_{OC}.

It is important to note that the suppression of bimolecular recombination that results from air annealing occurs not only at the PbS QD/PCBM interface but also between QDs in the bulk PbS QD film. It has been shown that, due to the high dielectric constant of PbS, a wide depletion region (~150 nm) can form in the PbS QD film of a Schottky solar cell structure under short-circuit conditions. In our bilayer devices, the width of this depletion region will be reduced due to insertion of the PCBM layer, although it may still significantly contribute to the photocurrent. Therefore, at voltages lower than the open-circuit voltage (*i.e.*, before the depletion region width reaches zero), bimolecular recombination of charge carriers between QDs must also be taken into consideration in modeling of the electronic processes that govern device operation.

CONCLUSION

We fabricated PbS QD-based solar cells that incorporate PCBM as the electron-transporting/hole-blocking layer. By applying a simple two-step processing method consisting of air annealing and a post-annealing thiol treatment, we are able to modify the surface properties of the PbS QDs and consequently the performance of the solar cells. We show that the fill factor of the device is predominantly affected by the shunt resistance of the device, which can be enhanced by (1) using a bilayer structure and (2) creating a film morphology where QDs are surrounded by the less conductive oxide compounds that spatially separate photogenerated charges, inhibiting their recombination, and leading to increased V_{OC}. Presently, the power conversion efficiency of the air-annealed devices is limited by the low photocurrent, which is largely due to the low optical absorption and the high series resistance of the QD films. The field dependence of the photocurrent in these structures appears to be dominated by charge transfer and charge recombination processes and is less affected by charge transport. These insights demonstrate the importance of limiting current leakage and interfacial charge recombination in QD solar cells (which is reflected in the high shunt resistance and late turn-on in the forward bias) and suggest that introduction of an inert interfacial layer (such as that of PbO on PbS QDs) can assist in maintaining the high V_{OC} and FF.

METHODS

Materials. Lead(II) acetate trihydrate (PbAc), oleic acid (OA), hexamethyldisilathiane (TMS2-S), 1-octadecene (ODE), hexane, methanol, butanol, butylamine, ethanedithiol (EDT), and acetonitrile (all solvents are anhydrous) were purchased from Sigma-Aldrich and used as received. PCBM was purchased from American Dye Source Co. and used without additional purification.

Quantum Dots Synthesis and Ligand Exchange. The lead precursor was prepared by dissolving and degassing 11.380 g of PbAc in a mixture of 270 mL of OA and 30 mL of ODE at 100 °C. After the lead precursor was made, the solution was heated to 150 °C under argon, followed by the swift injection of the sulfur precursor formed with 3.15 mL of TMS2-S and 150 mL of ODE. After synthesis, the QDs were purified and extracted with a mixture of methanol and butanol and then redispersed in hexane. Finally, the QDs were washed twice with methanol and stored as a powder.

The ligand exchange was performed inside a nitrogen glovebox by dispersing the OA capped QDs in butylamine. After 3 days, the QDs were precipitated with methanol and redispersed in octane to achieve a typical concentration of 75 mg/mL.

Device Fabrication. The patterned indium tin oxide (ITO)-coated glass substrates were treated in 0.2 M (3-mercaptopropyl)trimethoxysilane (MPTMS, in toluene) solution for 12 h to grow a self-assembled monolayer of MPTMS, for the purpose of improving the adhesion of the QD films on the substrates. After the treatment, the PbS QD solution was spin-coated on the substrates at 1500 rpm for 1 min. The QD films were then dipped in 0.002 M EDT (in acetonitrile) solution for 30 s, followed by a rinse with pure acetonitrile. The spin coating and EDT treatment procedure was repeated twice to achieve a film thickness of approximately 110 nm. We also experimented with a layer-by-layer dip coating technique[25] to make PbS QD films from the OA capped QD solution. For the air-annealed devices, the two deposition methods yield almost identical device characteristics. For the pristine devices, however, the dip coating method generally results in lower fill factor and slightly lower short-circuit current (see Figure S5 in Supporting Information). We note that film morphology of all the QD thin films appeared similar in atomic force microscopy images. Following oxidation and ligand exchange treatments of the PbS QD layer, a ~70 nm thick PCBM layer is spin-coated from a 10 mg/mL PCBM solution in chloroform. Finally, the top electrode was deposited by evaporation of 50 nm thick film of Mg followed by 70 nm thick film of Ag. Each device has an area of 0.012 cm^2.

Characterization. The current−voltage characteristics of the devices were measured using either a Keithley 6487 sourcemeter or a HP 4155B semiconductor parameter analyzer. The devices were illuminated through the glass substrate using an Oriel 91191 1000 W full spectrum solar simulator. Spectral mismatch was not corrected for these measurements. For the light intensity dependence experiment, devices were illuminated with a Newport LPM laser diode (λ = 1310 nm) in conjunction with a variable neutral density filter wheel to control the light intensity. For the carrier recombination lifetime measurement, a Newport LQD laser diode (λ = 1310 nm) driven by an Agilent 33220A function generator was used as a second light source to provide square wave modulated illumination. This illumination was filtered through a neutral density filter before reaching the device to ensure a small illumination perturbation. V_{OC} decay transients were recorded on a Tektronix TDS 3054B digital oscilloscope with a Tektronix ADA440A high impedance differential preamplifier. The X-ray photoelectron spectroscopy was carried out using a Kratos Axis Ultra spectrometer equipped with a monochromated Al Kα X-rays (1486.6 eV) operating at 150 W power. The optical absorption spectra of PbS QD films were obtained by measuring the transmittance of the films on glass substrates, using a Cary 5E UV−vis−NIR dual-beam spectrophotometer. For the external quantum efficiency spectrum measurements, the incident light was generated by a quartz tungsten halogen lamp, chopped at 45 Hz, dispersed by a monochromator, and conducted through an optical fiber to the sample surface. The light intensity was calibrated using a combination of a Newport silicon photodetector (for wavelength of 400−800 nm) and a germanium photodetector (for wavelength of 800−1500 nm), and the photocurrent at a short-circuit condition was measured with a Stanford Research SR830 lock-in amplifier.

Acknowledgment. This work was supported by the Department of Energy Solar America Program. The authors thank the Center of Materials Science and Engineering (CMSE) at MIT for providing the shared testing facilities used in this work, Dr. Scott Speakman at CMSE for performing the X-ray diffraction measurements, and Ms. Elisabeth Shaw for her assistance in the X-ray photoelectron spectroscopy. T.P.O. gratefully acknowledges support from the National Science Foundation Graduate Research Fellowship Program and the Link Foundation. M.T.B. thanks the Fondazione Fratelli Rocca for financial support through the Progetto Rocca fellowship.

Supporting Information Available: FET and X-ray diffraction data for PbS QD films. This material is available free of charge *via* the Internet at http://pubs.acs.org.

REFERENCES AND NOTES

1. Tang, C. W. 2-Layer Organic Photovoltaic Cell. *Appl. Phys. Lett.* **1986**, *48*, 183–185.
2. Peumans, P.; Uchida, S.; Forrest, S. R. Efficient Bulk Heterojunction Photovoltaic Cells Using Small-Molecular-Weight Organic Thin Films. *Nature* **2003**, *425*, 158–162.
3. Peumans, P.; Yakimov, A.; Forrest, S. R. Small Molecular Weight Organic Thin-Film Photodetectors and Solar Cells. *J. Appl. Phys.* **2003**, *93*, 3693–3723.

4. Xue, J. G.; Uchida, S.; Rand, B. P.; Forrest, S. R. 4.2% Efficient Organic Photovoltaic Cells with Low Series Resistances. *Appl. Phys. Lett.* **2004**, *84*, 3013–3015.
5. Chen, H.-Y.; Hou, J.; Zhang, S.; Liang, Y.; Yang, G.; Yang, Y.; Yu, L.; Wu, Y.; Li, G. Polymer Solar Cells with Enhanced Open-Circuit Voltage and Efficiency. *Nat. Photonics* **2009**, *3*, 649–653.
6. Giebeler, C.; Marks, R. N.; Bleyer, A.; Bradley, D. D. C.; Schrader, S. The Photovoltaic Effect in Poly(*p*-phenylene-2,3′-bis(3,2′-diphenyl)-quinoxaline-7-7′-diyl). *Opt. Mater.* **1998**, *9*, 99–103.
7. Halls, J. J. M.; Walsh, C. A.; Greenham, N. C.; Marseglia, E. A.; Friend, R. H.; Moratti, S. C.; Holmes, A. B. Efficient Photodiodes from Interpenetrating Polymer Networks. *Nature* **1995**, *376*, 498–500.
8. Li, G.; Shrotriya, V.; Huang, J. S.; Yao, Y.; Moriarty, T.; Emery, K.; Yang, Y. High-Efficiency Solution Processable Polymer Photovoltaic Cells by Self-Organization of Polymer Blends. *Nat. Mater.* **2005**, *4*, 864–868.
9. Park, S. H.; Roy, A.; Beaupre, S.; Cho, S.; Coates, N.; Moon, J. S.; Moses, D.; Leclerc, M.; Lee, K.; Heeger, A. J. Bulk Heterojunction Solar Cells with Internal Quantum Efficiency Approaching 100%. *Nat. Photonics* **2009**, *3*, 297–303.
10. Gur, I.; Fromer, N. A.; Geier, M. L.; Alivisatos, A. P. Air-Stable All-Inorganic Nanocrystal Solar Cells Processed from Solution. *Science* **2005**, *310*, 462–465.
11. Huynh, W. U.; Dittmer, J. J.; Alivisatos, A. P. Hybrid Nanorod−Polymer Solar Cells. *Science* **2002**, *295*, 2425–2427.
12. Alivisatos, A. P. Semiconductor Clusters, Nanocrystals, and Quantum Dots. *Science* **1996**, *271*, 933–937.
13. Murray, C. B.; Norris, D. J.; Bawendi, M. G. Synthesis and Characterization of Nearly Monodisperse CdE (E = S, Se, Te) Semiconductor Nanocrystallites. *J. Am. Chem. Soc.* **1993**, *115*, 8706–8715.
14. Dabbousi, B. O.; RodriguezViejo, J.; Mikulec, F. V.; Heine, J. R.; Mattoussi, H.; Ober, R.; Jensen, K. F.; Bawendi, M. G. (CdSe)ZnS Core−Shell Quantum Dots: Synthesis and Characterization of a Size Series of Highly Luminescent Nanocrystallites. *J. Phys. Chem. B* **1997**, *101*, 9463–9475.
15. Luther, J. M.; Law, M.; Beard, M. C.; Song, Q.; Reese, M. O.; Ellingson, R. J.; Nozik, A. J. Schottky Solar Cells Based on Colloidal Nanocrystal Films. *Nano Lett.* **2008**, *8*, 3488–3492.
16. Barkhouse, D. A. R.; Pattantyus-Abraham, A. G.; Levina, L.; Sargent, E. H. Thiols Passivate Recombination Centers in Colloidal Quantum Dots Leading to Enhanced Photovoltaic Device Efficiency. *ACS Nano* **2008**, *2*, 2356–2362.
17. Johnston, K. W.; Pattantyus-Abraham, A. G.; Clifford, J. P.; Myrskog, S. H.; MacNeil, D. D.; Levina, L.; Sargent, E. H. Schottky-Quantum Dot Photovoltaics for Efficient Infrared Power Conversion. *Appl. Phys. Lett.* **2008**, *92*, 151115.
18. Koleilat, G. I.; Levina, L.; Shukla, H.; Myrskog, S. H.; Hinds, S.; Pattantyus-Abraham, A. G.; Sargent, E. H. Efficient, Stable Infrared Photovoltaics Based on Solution-Cast Colloidal Quantum Dots. *ACS Nano* **2008**, *2*, 833–840.
19. Nelson, J. *The Physics of Solar Cells*; Imperial College Press: London, 2003.
20. Choi, J. J.; Lim, Y. F.; Santiago-Berrios, M. B.; Oh, M.; Hyun, B. R.; Sun, F.; Bartnik, A. C.; Goedhart, A.; Malliaras, G. G.; Abrua, H. D.; Wise, F. W.; Hanrath, T. PbSe Nanocrystal Excitonic Solar Cells. *Nano Lett.* **2009**, *9*, 3749–3755.
21. Leschkies, K. S.; Beatty, T. J.; Kang, M. S.; Norris, D. J.; Aydil, E. S. Solar Cells Based on Junctions between Colloidal PbSe Nanocrystals and Thin ZnO Films. *ACS Nano* **2009**, *3*, 3638–3648.
22. Rauch, T.; Boberl, M.; Tedde, S. F.; Furst, J.; Kovalenko, M. V.; Hesser, G. N.; Lemmer, U.; Heiss, W.; Hayden, O. Near-Infrared Imaging with Quantum-Dot-Sensitized Organic Photodiodes. *Nat. Photonics* **2009**, *3*, 332–336.
23. Szendrei, K.; Cordella, F.; Kovalenko, M. V.; Boberl, M.; Hesser, G.; Yorema, M.; Jarzab, D.; Mikhnenko, O. V.; Gocalinska, A.; Saba, M.; Quochi, F.; Mura, A.; Bongiovanni, G.; Blom, P. W. M.; Heiss, W. G.; Loi, M. A. Solution-Processable Near-IR Photodetectors Based on Electron Transfer from PbS Nanocrystals to Fullerene Derivatives. *Adv. Mater.* **2009**, *21*, 683–687.
24. Klem, E. J. D.; Shukla, H.; Hinds, S.; MacNeil, D. D.; Levina, L.; Sargent, E. H. Impact of Dithiol Treatment and Air Annealing on the Conductivity, Mobility, and Hole Density in PbS Colloidal Quantum Dot Solids. *Appl. Phys. Lett.* **2008**, *92*, 212105.
25. Luther, J. M.; Law, M.; Song, Q.; Perkins, C. L.; Beard, M. C.; Nozik, A. J. Structural, Optical, and Electrical Properties of Self-Assembled Films of PbSe Nanocrystals Treated with 1,2-Ethanedithiol. *ACS Nano* **2008**, *2*, 271–280.
26. Klem, E. J. D.; MacNeil, D. D.; Levina, L.; Sargent, E. H. Solution Processed Photovoltaic Devices with 2% Infrared Monochromatic Power Conversion Efficiency: Performance Optimization and Oxide Formation. *Adv. Mater.* **2008**, *20*, 3433–3439.
27. Tang, J.; Brzozowski, L.; Barkhouse, D. A. R.; Wang, X.; Debnath, R.; Wolowiec, R.; Palmiano, E.; Levina, L.; Pattantyus-Abraham, A. G.; Jamakosmanovic, D.; Sargent, E. H. Quantum Dot Photovoltaics in the Extreme Quantum Confinement Regime: The Surface-Chemical Origins of Exceptional Air- and Light-Stability. *ACS Nano* **2010**, *4*, 869–878.
28. Konstantatos, G.; Levina, L.; Fischer, A.; Sargent, E. H. Engineering the Temporal Response of Photoconductive Photodetectors *via* Selective Introduction of Surface Trap States. *Nano Lett.* **2008**, *8*, 1446–1450.
29. Leatherdale, C. A.; Bawendi, M. G. Observation of Solvatochromism in CdSe Colloidal Quantum Dots. *Phys. Rev. B* **2001**, *63*, 165315.
30. Mihailetchi, V. D.; Wildeman, J.; Blom, P. W. M. Space-Charge Limited Photocurrent. *Phys. Rev. Lett.* **2005**, *94*, 126602.
31. O'Regan, B. C.; Scully, S.; Mayer, A. C.; Palomares, E.; Durrant, J. The Effect of Al_2O_3 Barrier Layers in TiO_2/Dye/CuSCN Photovoltaic Cells Explored by Recombination and DOS Characterization Using Transient Photovoltage Measurements. *J. Phys. Chem. B* **2005**, *109*, 4616–4623.
32. Goh, C.; Scully, S. R.; McGehee, M. D. Effects of Molecular Interface Modification in Hybrid Organic−Inorganic Photovoltaic Cells. *J. Appl. Phys.* **2007**, *101*, 114503.
33. Snaith, H. J.; Moule, A. J.; Klein, C.; Meerholz, K.; Friend, R. H.; Gratzel, M. Efficiency Enhancements in Solid-State Hybrid Solar Sells *via* Reduced Charge Recombination and Increased Light Capture. *Nano Lett.* **2007**, *7*, 3372–3376.